Cross-Hierarchical Transduction of Dynamic Behaviors from Self-Oscillating Microgels to Colloidosomes

*Zhouna Tang[1], Takafumi Enomoto[1], Takeshi Ueki[2,3], Ryota Tamate[2], Aya M. Akimoto[4], and Ryo Yoshida[1]**

[1]Department of Materials Engineering, School of Engineering, The University of Tokyo

7-3-1 Hongo, Bunkyo-ku, Tokyo 113-8656, Japan

[2]National Institute for Materials Science

1 Namiki, Tsukuba, Ibaraki 305-0044, Japan

[3]Graduate School of Life Science, Hokkaido University

Kita 10, Nishi 8, Kita-ku, Sapporo, Hokkaido, 060-0810, Japan

[4]Department of Human-Centered Engineering, Faculty of Transdisciplinary Engineering, Ochanomizu University

2-1-1 Ohtsuka, Bunkyo-ku, Tokyo 112-8610, Japan

ABSTRACT

Life consists of many hierarchical levels, in which complex behaviors emerge from the interactions among simpler components. Here we demonstrate the cross-hierarchical transduction of dynamic behaviors in life-like autonomous materials by investigating self-oscillating colloidosomes as a model system. Self-oscillating colloidosomes are composed of self-oscillating microgels, which exhibit autonomous flocculation/dispersion oscillation driven by a self-promoted Belouzov-Zhabotinsky reaction at certain temperatures. We identified chemo-mechanical transduction across hierarchical levels in self-oscillating colloidosomes under out-of-equilibrium conditions. The self-oscillating colloidosomes exhibited swelling/deswelling or shape deformation oscillations in a stochastic manner, originating from flocculation/dispersion oscillation at the microgel level. We found that the choice between these two oscillation modes is determined by the oscillation modes of their constituent self-oscillating microgels. These findings pave the way for cross-hierarchical design of chemically powered autonomous materials.

Introduction

Life is hierarchically organized, and each level has distinct functions and emergent properties. At the molecular level, small molecules and proteins respond to external stimuli, modulating the properties of their assembly states and thereby inducing the dynamic behaviors at the cellular level[1–3]. For example, the intracellular signal leads to actin polymerization and actomyosin contraction, thereby producing amoeboid migration of cells[4]. Understanding chemo-mechanical transduction across hierarchical levels is key to engineering dynamic behavior of chemically powered autonomous materials.

To create life-like autonomous materials, we have established the concept of self-oscillating polymer systems that exhibits dynamic behavior driven by self-promoted Belousov-Zhabotinsky (BZ) reaction[5]. The systems are mainly composed of thermoresponsive poly(*N*-isopropylacrylamide) (PNIPAAm) main chain and tris(2,2'-bipyridyl)ruthenium complex ($Ru(bpy)_3^{2+}$), a catalyst of the BZ reaction. Since the hydrophilicity of the self-oscillating polymers is different between the reduced state ($Ru(bpy)_3^{2+}$) and the oxidized state ($Ru(bpy)_3^{3+}$), the lower critical solution temperature (LCST) also differs in each state. Therefore, between a certain temperature range, these self-oscillating polymers undergo autonomous structural oscillations driven by the self-promoted BZ reaction. To date, we have developed several forms of self-oscillating materials, including gels[6–8], micelles and vesicles[9–11], and microgels[12,13]. Based on this driving mechanism, the self-oscillating materials provide a platform for investigating the cross-hierarchical transduction of chemical events.

In this context, we employed self-oscillating colloidosomes (SOCs) as a model system of hierarchical autonomous materials. Colloidosomes are cell-like spherical hollow structures[14], and are formed from Pickering emulsions that are stabilized by the self-assembly of amphiphilic colloid particles at the oil-water interface[15]. Because of their structures and flexible cell-like membranes, they are favored as simplified artificial cell models. Many studies have shown that silica particles[16–18] and polystyrene latex particles[19,20] can be used to fabricate the colloidosome structures. Recently, microgels have attracted increasing interest as emulsifiers for Pickering emulsions because of their unique deformability and stimuli responsiveness[21–25]. Our previous study demonstrated that SOCs composed of microgels exhibited periodic autonomous shape deformation in the presence of the BZ substrates[26].

In this study, we investigated chemo-mechanical transduction of dynamic behaviors in SOCs across two hierarchical levels, from microgels to colloidosomes (**Scheme 1**). By modifying the synthesis protocol for SOCs, we enabled independent characterization of the SOCs and their constituent self-oscillating microgels (SOMGs). We found that the thermoresponsive behaviors of the SOCs are inherited from the constituent SOMGs. Moreover, the dynamic behaviors of SOMGs were transduced into that of the SOCs under out-of-equilibrium conditions. At the microgel level, chemical redox oscillations of the $Ru(bpy)_3$ complex were transduced into mechanical oscillations between flocculated and dispersed states. Upon crosslinking SOMGs to form colloidosomes, these oscillations were further transduced into swelling/deswelling or shape deformation oscillations. In addition, the temperature dependence of SOC oscillations modes was inherited their constituent SOMGs. These results established that the dynamic characteristics of the lower hierarchy were transduced to the higher hierarchy.

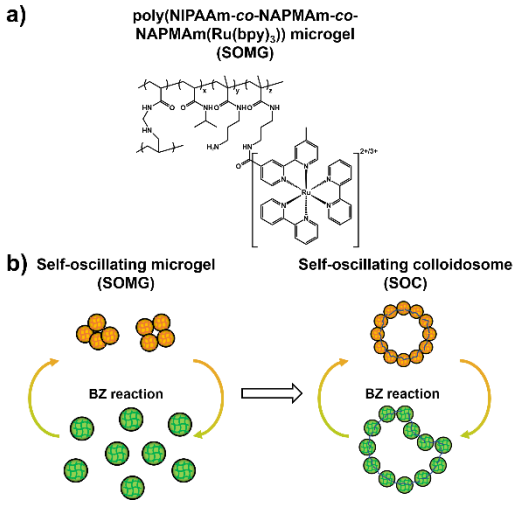

Scheme 1. (a) Chemical structure of poly(NIPAAm-*co*-NAPMAm-*co*-NAPMAm($Ru(bpy)_3$)) microgel (SOMG). (b) Schematic illustration of self-oscillating colloidosomes (SOCs) assembled by self-oscillating microgels (SOMGs).

Experimental section

Materials. *N*-Isopropylacrylamide (NIPAAm) was generously donated by the KJ chemicals Co. (Tokyo, Japan), and purified by recrystallization from toluene/hexane mixed solvent. *N*-(3-Aminopropyl)methacrylamide hydrochloride (NAPMAm) was purchased from Combi-Blocks (San Diego, USA), and purified by reprecipitation in Tetrahydrofura. *N*-Succinimidyl acrylate (NAS) was purchased from Tokyo Chemical Industry (Tokyo, Japan). Potassium peroxydisulfate (KPS) was purchased from Kanto Chemical (Tokyo, Japan). *N,N*-Dimethylacrylamide (DMAAm) was purchased from FUJIFILM Wako Pure Chemical Co. (Osaka, Japan), and was purified by being passed through a column of basic alumina before using. Bis(2,2'-bipyridine)(1-(4'-methyl-2,2'-bipyridine-4-carbonyloxy)-2,5-pyrrolidinedione)-ruthenium(II) bis(hexafluorophosphate) (NHH-Ru(bpy)$_3$) was purchased from HangZhou Trylead Chemical Technology (Hangzhou, China). All other chemical reagents were purchased from Wako Pure Chemical Corporation, and used as received.

Synthesis of poly(NIPAAm-*co*-NAS). Poly(NIPAAm-*co*-NAS) was synthesized by free radical polymerization. NIPAAm (5.04 g, 44.6 mmol), NAS (0.381 g, 2.26 mmol), and 2,2'-azobis(isobutyronitrile) (AIBN) (34.8 mg, 0.212 mmol) were added into a 100 mL three-neck round-bottom flask and methanol (30 mL) was added as a solvent. DMF (774 μL, 10.0 mmol) was also added into the reaction solution as the NMR calculation standard. The solution was deoxygenated by argon gas bubbling at room temperature for 30 min. The polymerization was carried out at 60 °C for 24 h. The reaction was quenched by cooling down in an ice-water bath. The reacted solution was evaporated by a rotary evaporator and was dissolved in a good solvent, the mixture of toluene and acetone, and then was reprecipitated in a poor solvent, hexane. After

the suction filtration, the collected powders were redissolved into the mixture of toluene and acetone, and then the reprecipitation in hexane was carried out. The collected polymers were dried under vacuum for 48 h. Finally, white solid products were obtained. Poly(DMAAm-*co*-NAS) was synthesized by the same procedure except the monomers were changed from NIPAAm to DMAAm.

Synthesis of poly(NIPAAm-*co*-NAPMAm) microgel. poly(NIPAAm-*co*-NAPMAm) microgels were synthesized by precipitation polymerization. NIPAAm (1.69 g, 14.9 mmol), NAPMAm (0.268 g, 1.50 mmol), and *N,N'*-methylenebis(acrylamide) (MBAAm) (0.0568 g, 0.368 mmol) were added into a 300 mL three-neck round-bottom flask and deionized water (95 mL) was added as a solvent. DMF (774 μL, 10.0 mmol) was also added into the reaction solution as the NMR calculation standard. The solution was deoxygenated by argon gas bubbling at 70 °C for 30 min. KPS (0.0405 g, 0.150 mmol) was added into a 13.5 mL screw bottle and dissolved in deionized water (5 mL). The initiator solution was deoxygenated by argon gas bubbling at room temperature for 30 min. Then, the initiator solution was added into the flask through a PTFE tube. The reaction was carried out at 70 °C for 1 h and the solution was stirred at 250 rpm during the reaction. The reaction was quenched at room temperature with an open atmosphere. The reacted solution was dialyzed against deionized water, and the dialysis solvent was exchanged one time. Finally, white solid products were obtained by a freeze-dryer.

Synthesis of poly(NIPAAm-*co*-NAPMAm-*co*-NAPMAmRu(bpy)$_3$) microgel (SOMG). 0.95 g of poly(NIPAAm-*co*-NAPMAm) microgel was dissolved into 50 mL of DMSO, and then NHS-Ru(bpy)$_3$ (370 mg, 0.365 mmol), and triethylamine (TEA) (305 μL, 2.19 mmol) were also added.

The reaction was carried out at room temperature for 24 h. The solution was dialyzed against DMSO, and the dialysis solvent was exchanged twice. Then, the dialysis solvent was changed to deionized water, and was exchanged four times. Finally, orange solid products were obtained by a freeze-dryer.

Fabrication of colloidosome. The fabrication scheme is shown in **Scheme S1**. 200 mg of P(NIPAAm-*co*-NAPMAm-*co*-NAPMAmRu(bpy)$_3$) microgel was dissolved into 5 mL of PBS(-), and 100 mg of poly(NIPAAm-*co*-NAS) was dissolved into another 5 mL of PBS(-). Then, two solutions were fully mixed. Next, 40 mL of 1-octanol was added into the mixed solution, and the solution was vigorously mixed. The resulted dispersion was left overnight at 20 ℃ for the cross-linking reaction. Next day, the supernatant oil was eliminated, and 20 mL of ethanol was added to dissolve the oil and water. After the colloidosomes precipitated in the bottle, the supernatant was eliminated again, and 20 mL of ethanol was added. Next, the solution was dialyzed against ethanol, and the dialysis solvent was exchanged twice. Then, the dialysis solvent was changed to deionized water, and was exchanged three times. Finally, the colloidosomes were stored in the solution for the following experiments. The colloidosomes whose crosslinkers were P(DMAAm-*co*-NAS), were fabricated with the same procedure.

Dynamic light scattering (DLS) measurement. DLS measurements were carried out on a zeta-potential & particle size analyzer (Otsuka ELSZ–2000, Japan). The sample solution was equilibrated for 10 min at each temperature. The hydrodynamic radius (R_h) was calculated using the CONTIN analysis.

UV-vis absorption measurement. UV-vis measurement was carried out on a UV-vis spectrophotometer (SHIMADZU UV-1900i, Japan) with a thermoelectric cell holder (SHIMADZU S-1700, Japan). For the measurement of oscillatory behaviors, the time course mode was used. The wavelength was set as a certain wavelength and the measurement time was set as 3600 s.

Optical microscopic observation. The microscopic observation was conducted on the digital microscope (Keyence, VHX-900, Japan) equipped with a high-resolution 1000x zoom lens (Keyence, VH-Z100R). A 24 mm × 24 mm glass slide (thickness: 0.12 – 0.17 mm) was used for holding the sample solution. An appropriate size circle was drawn on the glass slide using high vacuum grease to avoid the leakage of the solution. Then, the sample solution was added to the circular range and another glass slide was used as a cover.

Confocal microscopic observation. Confocal laser scanning microscopy was conducted using FLUOVIEW FV3000 Confocal Microscope (Olympus, Japan) with a 100× oil immersion objective lens and a differential interference contrast (DIC) prism. The lens was immersed in oil (IMMOIL-F30CC, Olympus, Japan) to obtain clear image. The excitation wavelength was 488 nm. A 24 mm × 24 mm glass slide (thickness: 0.12 – 0.17 mm) was used for holding the sample solution. An appropriate size circle was drawn on the glass slide using high vacuum grease to avoid the leakage of the solution. Then, the sample solution was added to the circular range and another glass slide was used as a cover.

Results and discussion

The microgels were synthesized by the precipitation copolymerization of NIPAAm and NAPMAm. Then, BZ catalyst was introduced into the microgels to fabricate SOMGs through a condensation reaction between the NHS esters of $Ru(bpy)_3$ complex and the primary amine groups of NAPMAm units. According to the previous study, by using 1-octanol as the oil phase, it is possible to fabricate the water-in-oil (W/O) Pickering emulsion stabilized by PNIPAAm microgels[27]. Based on this procedure, we fabricated the colloidosome structures using SOMGs through the W/O emulsion method. The polymer crosslinker, poly(NIPAAm-*co*-NAS), was used to maintain the colloidosome structure after redispersing into the aqueous solution. After the dialysis, the obtained SOCs were stored in the aqueous solution.

First, we examined the internal structure of the SOCs, which are assembled from the SOMGs. Because of the phosphorescence of the $Ru(bpy)_3$ complex, the internal structure of the SOCs could be visualized using the confocal laser scanning microscopy. **Figure 1** shows that the SOCs have a hollow structure with a membrane thickness around 2-3 μm. According to the DLS results, R_h of the SOMGs is around 635 nm in water at 24 ℃ (**Figure S1**). These results suggest that the membrane of the SOCs is not composed of a monolayer of the SOMGs. A similar phenomenon was also reported in a previous study using 1-octanol as the oil phase in the W/O emulsion method[27]. Uptake of 1-octanol by microgels increases the attractive interaction between microgels, resulting in greater adsorption at the interface layer and formation of heterogeneous membranes. We also assumed that the size distribution of the SOMG and the broad molecular weight distribution of the polymer crosslinker contributed to the inhomogeneity of the membrane (**Figure S2a**).

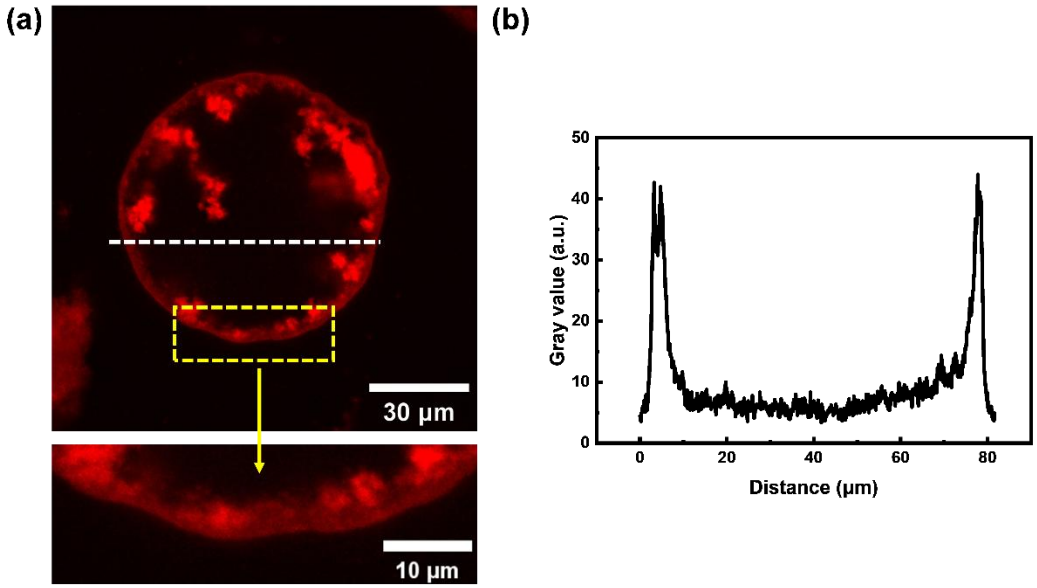

Figure 1. (a) Confocal microscopic image of single SOC and the zoom in part of the membrane of the SOC (yellow dash line rectangle). (T = 24 ºC, solvent: water) (b) Plot correspond to the intensity profile along the white respective dash line on the confocal image.

The thermoresponsive behaviors of the SOMGs were then studied. In high salt concentration solutions, PNIPAAm microgels aggregate above a certain temperature due to increased hydrophobicity of the microgel network[28]. This temperature is determined as critical flocculation temperature (CFT). **Figure 2** shows the temperature dependence of the SOMG dispersion from DLS measurements under reduced and oxidized conditions. The hydrodynamic radius (R_h) increases sharply above a specific temperature in each case, indicating the CFTs for reduced and oxidized states at $T_{F,red}$ = 15 ºC and $T_{F,ox}$ = 25 ºC, respectively. We also found that the R_h of the oxidized state is bigger than that of the reduced state below the $T_{F,red}$, which is attributed to the higher hydrophilicity of SOMGs in the oxidized state. In addition, the SOMG was slightly shrunk as the temperature increased below the T_F, which is attributed to the thermoresponsive volume phase transition of PNIPAAm based microgels, similar to a previous report[29].

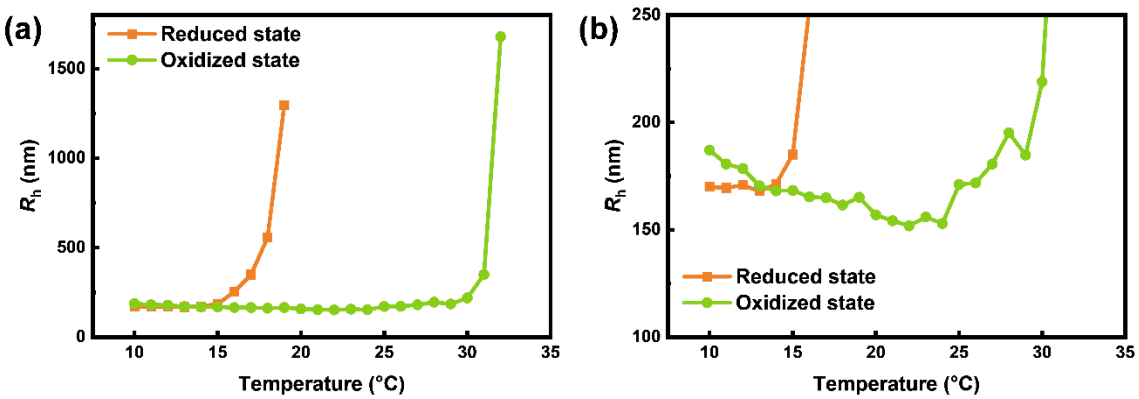

Figure 2. (a) Temperature dependence of the hydrodynamic radius (R_h) for the SOMG dispersions under reduced and oxidized conditions, and (b) enlarged view of panel (a). ([SOMG] = 0.5 g/L, reduced condition: [HNO_3] = 800 mM, [NaCl] = 50 mM; oxidized condition: [HNO_3] = 800 mM, [$NaBrO_3$] = 50 mM)

The equilibrium swelling ratio for the SOCs under both reduced and oxidized conditions were also determined, with the projected area at 10 °C normalized to 1 (**Figure 3**). As the temperature increased, the equilibrium swelling ratio gradually decreased, indicating the deswelling of the SOCs. One of the reasons for this phenomenon is the thermoresponsiveness of the SOMGs, the main component of the SOCs. Although the SOMGs on the SOCs are fixed by the polymer crosslinker and cannot move freely, they still tend to move closer together due to the flocculation above the CFT, leading to deswelling of the SOCs. Additionally, consistent with the volume phase transition behavior of self-oscillating gels[6], the SOMGs also deswell with increasing temperature under the CFT as shown in **Figure 2b**, thereby contributing to the deswelling of the SOCs. Note that thermoresponsive deswelling was also observed for the SOCs crosslinked with the non-thermoresponsive polymer, poly(DMAAm-*co*-NAS) (**Figure S3**), indicating that the deswelling and flocculation at the microgel level are transduced into deswelling at the colloidosome level.

Another reason comes from the thermoresponsive property of the polymer crosslinker poly(NIPAAm-*co*-NAS), which has a lower critical solution temperature (LCST) at 20 ºC (**Figure S2b**). Contraction of the crosslinker polymer chains shortens the distance between microgels, leading to a more compact structure. As a result, the temperature dependent deswelling of the SOCs arises from both the thermoresponsive property of the SOMGs and the crosslinker. In addition, the swelling ratio of the SOCs also differs between redox states (**Figure 3**). This arises from differences in the flocculation temperatures of the constituent SOMGs in redox states ($T_{F,red} < T_{F,ox}$). Overall, these results clearly indicate that the thermoresponsive behaviors of the SOMGs were successfully inherited by the SOCs.

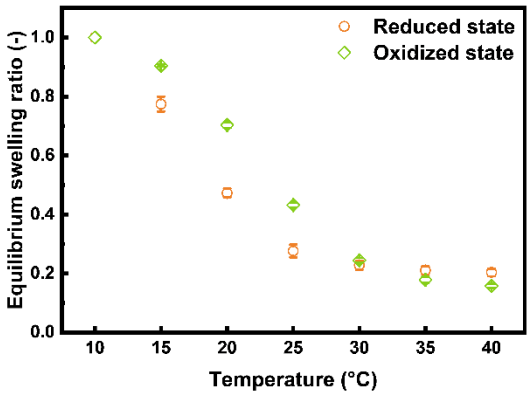

Figure 3. Equilibrium swelling ratio of the SOC under the reduced and oxidized conditions. The values are the average of three different SOCs. (reduced condition: [HNO_3] = 800 mM, [NaCl] = 50 mM; oxidized condition: [HNO_3] = 800 mM, [$NaBrO_3$] = 50 mM)

Thus far, we have investigated the thermoresponsive behaviors of the SOMGs and SOCs. We next focus on dynamic chemo-mechanical transduction under out-of-equilibrium conditions. Since the flocculation of the SOMGs decreases the optical transmittance of their dispersions[30], the self-oscillating behaviors of the SOMGs can be observed by UV-vis absorption spectroscopy. The self-oscillating profiles at different temperatures were observed at 583 nm, an isosbestic point between

the reduced and oxidized SOMGs, as shown in **Figure 4a**. All samples exhibited periodic oscillations in optical transmittance, indicating the flocculation/dispersion oscillation of the SOMG driven by the BZ reaction. At 15 ℃, only slight flocculation occurred in the reduced state as shown in **Figure 2**. Consequently, the amplitude of the transmittance oscillations was much smaller than the other two temperatures. At 20 ℃, the SOMGs in the reduced state drastically flocculated, and a clear transmittance oscillation was observed. Note that the oscillation became unstable overtime, and transmittance did not completely recover to its initial value, which implies the incomplete dispersion of SMOGs during the oxidized regime. When the temperature was increased to 25 ℃, the optical transmittance decreased sharply at the outset, indicating the formation of large aggregates. However, the oscillation amplitudes at 25 ℃ were smaller than those at 20 ℃, because the SOMGs in the oxidized state already flocculated slightly at 25 ℃ (**Figure 2**), and redispersion during the oxidized regime was less complete. We also found that the SOMGs precipitated over time (**Figure S4**), leading to an increase in transmittance at the later times. Then, the average oscillation periods were calculated using the 4th to 8th cycles. As shown in **Figure 4b**, the average oscillation period decreased as the temperature increased, which is consistent to Arrhenius equation[31]. Based on these results, we speculate that the precipitation observed at 25 ℃ was induced by the faster oscillation rate at higher temperatures. The increased oscillation rate leads to a shorter oscillation period. During this period, the flocculated SOMGs in the reduced state lack sufficient time to fully disperse upon the oxidized regime. As a result, the SOMG dispersion oscillated between a flocculated reduced state and an incompletely dispersed oxidized state at 25 ℃.

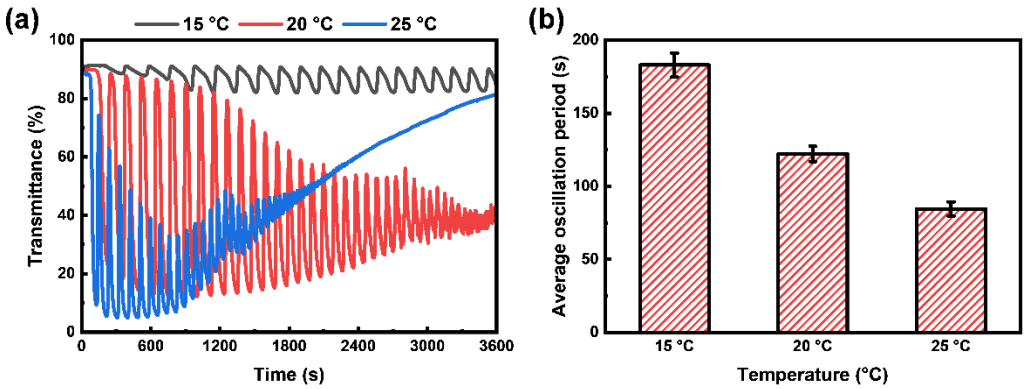

Figure 4. (a) Oscillation profiles of optical transmittance for the SOMG dispersions at different temperatures. (BZ reaction condition: [SOMG] = 0.38 g/L, [HNO_3] = 800 mM, [$NaBrO_3$] = 50 mM, [Malonic Acid] = 100 mM, wavelength: 583 nm) (b) Average oscillation period for the SOMG dispersions at different temperatures.

Next, we examined the self-oscillating behaviors of the SOCs. At 20 ℃ in the presence of BZ substrates, the SOC exhibited the autonomous swelling/deswelling oscillations (**Figure 5a**, **Movie S1**). Because $Ru(bpy)_3$ catalysts are tethered only within the SOMGs, the constituent SOMGs drive these oscillations via the self-promoted BZ reaction. The redox oscillations induce flocculation/dispersion oscillation at microgel level, and these oscillations were transduced into volumetric oscillations at colloidosome level. This result is also consistent with a higher equilibrium swelling ratio of the SOCs in the oxidized state than in the reduced state.

Another mode of self-oscillations was also observed for the SOC at 20 ℃ in the presence of BZ substrates (**Figure 5b**, **Movie S2**). The shape of the SOC periodically changed between a circular shape and an irregular shape, that is the buckling/unbuckling shape deformation oscillation. This behavior is similar to our previous report[26]. Same as the swelling/deswelling oscillation mentioned above, the SOC tends to swell in the oxidized state during the BZ reaction. However, since the SOC is crosslinked, the volume change is restricted. Therefore, the membrane buckled inside to

accommodate swelling by increasing surface area. Upon returning to the reduced state, the SOC deswelled and recovered a circular shape. We discuss the occurrence of the volume and the shape deformation oscillations in the SOCs later.

Besides 20 ℃, the SOCs were also observed under 15 ℃ and 25 ℃. The self-oscillating profiles and movies were in the Supporting Information (**Figure S5-8** and **Movie S3-6**). The self-oscillating profile of the SOC that shows shape deformation was used for the calculation of the average oscillation period. **Figure 5c** shows that, when the reaction temperature increased, the average oscillation period of the SOC decreased, which is similar to the result of the SOMG dispersion. As a consequence, the self-oscillating behaviors of the SOC at different temperatures is also consistent to Arrhenius equation[31].

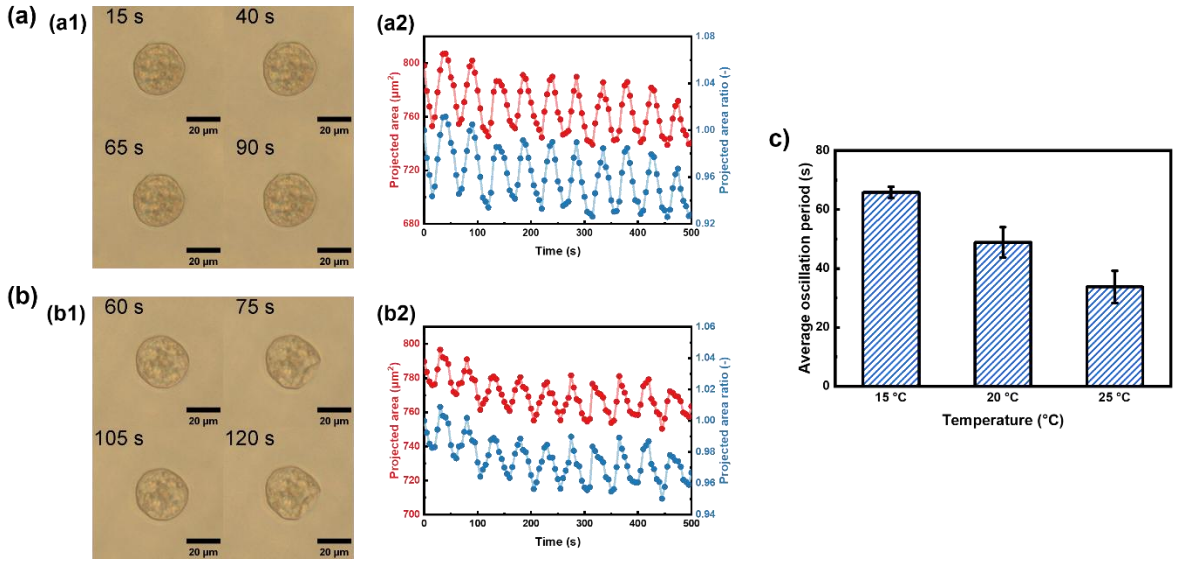

Figure 5. (a) Autonomous swelling/deswelling oscillation and (b) shape deformation oscillation of colloidosomes at 20 ℃ during the BZ reaction. (BZ reaction condition: [HNO_3] = 800 mM, [$NaBrO_3$] = 50 mM, [Malonic Acid] = 100 mM) (a1) (b1) Snapshots of the colloidosome at different moments under the optical microscope. (a2) (b2) Oscillation profiles of projected areas and projected area ratios for the colloidosome. The projected area ratio (-) is defined as the

296 projected area at time t normalized by the projected area at time t = 0. (c) Average oscillation
297 period for the SOC dispersion at different temperatures.

298 **Table 1** summarizes of the occurrence percentages for each oscillation mode at different
299 temperatures. The occurrence of the swelling/deswelling oscillation and the shape deformation
300 oscillation on SOCs appears random (**Table S1**), which may be attributed to the heterogeneity in
301 membrane thickness of the SOCs. Then, according to our previous study [26], larger SOCs exhibit
302 higher probability of shape deformation oscillations. As shown in **Table S1**, the SOCs had larger
303 diameters at 15 ℃ compared with those in higher temperature. However, the occurrence for shape
304 deformation oscillations was only 26.7%, which is less than that at 20 ℃, and the deformation
305 amplitude was small (**Figure S6** and **Movie S4**). These results are likely linked to the self-
306 oscillation behaviors of the SOMGs. At 15 ℃, the SOMGs exhibited autonomous oscillations
307 between dispersion and slight flocculation with small amplitudes (**Figure 4a**). We assumed that
308 the small flocculation/dispersion oscillation was transduced into the swelling/deswelling
309 oscillation in the SOCs with small amplitudes, leading to a lower probability of shape deformation
310 oscillations (**Figure 6a**). When the temperature was increased to 20 ℃, the average diameter for
311 the SOCs decreased compared to that at 15 ℃ (**Table S1**). On the other hand, deformation was
312 much more obvious, and the occurrence percentage of shape deformation oscillations increased.
313 This is likely because of the drastic transitions of the SOMGs between flocculation and dispersion
314 states at 20 ℃ (**Figure 4a**), thereby driving shape deformation oscillations of the SOCs across
315 hierarchy (**Figure 6b**). At 25 ℃, deformation on the SOCs became slight again (**Figure S8** and
316 **Movie S6**), and the occurrence percentage of deformation oscillations was lower than that at 20 ℃.
317 Additionally, nearly half of the SOCs did not show volumetric oscillations. As mentioned earlier,
318 the SOMG exhibited the flocculation/incomplete dispersion oscillations at 25 ℃ due to the higher

oscillation rate (**Figure 4a**). We speculated that the incomplete oscillation in the microgel level was transduced into smaller oscillation amplitudes in the colloidosome level (**Figure 6c**). Together, these observations indicate that the dynamic behaviors of the SOMGs are also inherited by the higher hierarchical level.

Table 1. Summary of the percentage of occurrence of each oscillation type at each temperature. 15 different colloidosomes were counted at each temperature. Conditions of BZ substrates were the same as **Figure 4**.

Temperature (℃)	No volume oscillation (%)	Swelling/deswelling oscillation (%)	Shape deformation oscillation (%)
15	0	73.3	26.7
20	0	53.3	46.7
25	46.7	33.3	20.0

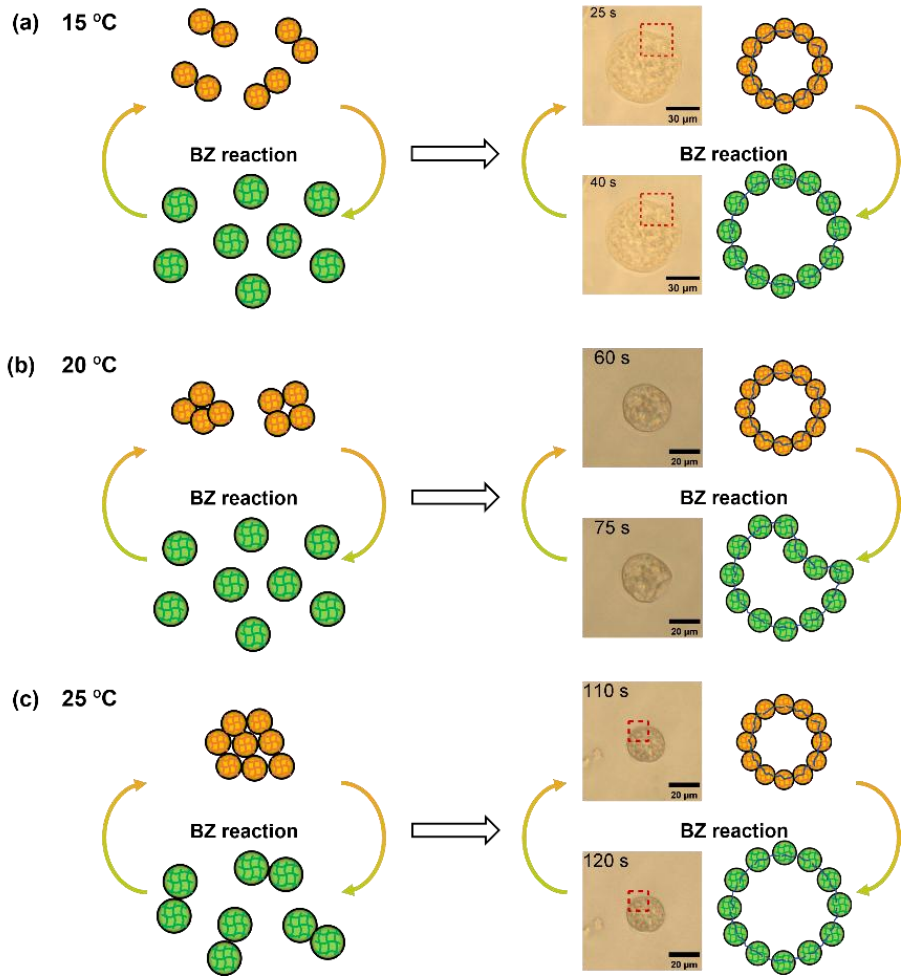

Figure 6. Schematic illustration of the self-oscillating behaviors of SOMGs and SOCs at (a) 15 ℃, (b) 20 ℃, and (c) 25 ℃.

Conclusion

In this study, the independent characterization of the SOMGs and the SOCs revealed the cross-hierarchical transduction of dynamic behaviors. This was realized by modifying the synthesis protocol, that is first synthesizing SOMGs and then fabricating SOCs using the SOMGs. Under equilibrium conditions, thermoresponsive deswelling and flocculation at the microgel level were transduced into deswelling at the colloidosome level. Beyond these thermoresponsive behaviors, dynamic behaviors under out-of-equilibrium conditions were also inherited across the hierarchy.

The SOMGs exhibited flocculation/dispersion oscillations driven by the self-promoted BZ reaction, and the oscillation modes depended on temperature. We found that flocculation/dispersion oscillation at the microgel level were transduced into the swelling/deswelling or shape deformation oscillations at the colloidosome level. Moreover, difference in the oscillation modes of the SOMGs determined the oscillation modes of the SOCs. These results show how dynamic behaviors are transduced from the lower hierarchical level, the SOMGs, to the higher hierarchical level, the SOCs. These findings pave the way for cross-hierarchical design of chemically powered autonomous materials via a bottom-up approach.

ASSOCIATED CONTENT

Additional experimental details, materials, and methods, including image of the SOMG dispersion, dynamic light scattering result of the microgel, GPC trace and the dynamic light scattering result of the polymer crosslinker, equilibrium swelling ratio of the SOC with the non-responsive crosslinker, self-oscillating profiles of the SOC during the BZ reaction at 15 and 25 °C, summary of the percentage of occurrence of each oscillation type at each temperature, Average diameter of SOCs at different temperatures (.PDF)

Video for the optical microscopic observation of the autonomous oscillation behaviors of the SOC during the BZ reaction (.mp4)

AUTHOR INFORMATION

Corresponding Author

Ryo Yoshida

Department of Materials Engineering, School of Engineering, The University of Tokyo, Tokyo, 113-8656, Japan; orcid.org/0000-0002-0558-2922; Email: ryo@cross.t.u-tokyo.ac.jp

Author Contributions

Conceptualization: ZT, TE, RY

Methodology: ZT

Investigation: ZT

Visualization: ZT

Supervision: TE, RY

Writing—original draft: ZT

Writing—review & editing: ZT, TE, TU, RT, AMA, RY

The manuscript was written through contributions of all authors. All authors have given approval to the final version of the manuscript.

Notes

The authors declare no competing financial interest.

ACKNOWLEDGMENT

This work was partially supported by Grants-in-Aid for Scientific Research Grant Numbers 24H00471, JP20H00388 and JP20K20563 to R.Y. from the Ministry of Education, Culture, Sports, Science, and Technology of Japan.

REFERENCES

(1) Lim, C. M.; Díaz, A. G.; Fuxreiter, M.; Pun, F. W.; Zhavoronkov, A.; Vendruscolo, M. Multiomic Prediction of Therapeutic Targets for Human Diseases Associated with Protein Phase Separation. *Proc. Natl. Acad. Sci. U. S. A.* **2023**, *120*, e2300215120.

(2) Saad, S.; Cereghetti, G.; Feng, Y.; Picotti, P.; Peter, M.; Dechant, R. Reversible Protein Aggregation Is a Protective Mechanism to Ensure Cell Cycle Restart after Stress. *Nat. Cell Biol.* **2017**, *19*, 1202–1213.

(3) Marijan, D.; Momchilova, E. A.; Burns, D.; Chandhok, S.; Zapf, R.; Wille, H.; Potoyan, D. A.; Audas, T. E. Protein Thermal Sensing Regulates Physiological Amyloid Aggregation. *Nat. Commun.* **2024**, *15*, 1222.

(4) Lämmermann, T.; Sixt, M. Mechanical Modes of "amoeboid" Cell Migration. *Curr. Opin. Cell Biol.* **2009**, *21*, 636–644.

(5) Yoshida, R. Creation of Softmaterials Based on Self-Oscillating Polymer Gels. *Polym. J.* **2022**, *54*, 827–849.

(6) Yoshida, R.; Takahashi, T.; Yamaguchi, T.; Ichijo, H. Self-Oscillating Gel. *J. Am. Chem. Soc.* **1996**, *118*, 5134–5135.

(7) Yoshida, R.; Takahashi, T.; Yamaguchi, T.; Ichijo, H. Self-Oscillating Gels. *Adv. Mater.* **1997**, *9*, 175–178.

(8) Maeda, S.; Hara, Y.; Sakai, T.; Yoshida, R.; Hashimoto, S. Self-Walking Gel. *Adv. Mater.* **2007**, *19*, 3480–3484.

(9) Ueki, T.; Shibayama, M.; Yoshida, R. Self-Oscillating Micelles. *Chem. Commun.* **2013**, *49*, 6947–6949.

(10) Tamate, R.; Ueki, T.; Shibayama, M.; Yoshida, R. Self-Oscillating Vesicles: Spontaneous Cyclic Structural Changes of Synthetic Diblock Copolymers. *Angew. Chem., Int. Ed.* **2014**, *53*, 11248–11252.

(11) Tamate, R.; Ueki, T.; Yoshida, R. Self-Beating Artificial Cells: Design of Cross-Linked Polymersomes Showing Self-Oscillating Motion. *Adv. Mater.* **2015**, *27*, 837–842.

(12) Suzuki, D.; Sakai, T.; Yoshida, R. Self-Flocculating/Self-Dispersing Oscillation of Microgels. *Angew. Chem., Int. Ed.* **2008**, *47*, 917–920.

(13) Suzuki, D.; Kobayashi, T.; Yoshida, R.; Hirai, T. Soft Actuators of Organized Self-Oscillating Microgels. *Soft Matter* **2012**, *8*, 11447–11449.

(14) Park, J. H.; Galanti, A.; Ayling, I.; Rochat, S.; Workentin, M. S.; Gobbo, P. Colloidosomes as a Protocell Model: Engineering Life-Like Behaviour through Organic Chemistry. *Eur. J. Org. Chem.* **2022**, *2022*, e202200968.

(15) Thompson, K. L.; Williams, M.; Armes, S. P. Colloidosomes: Synthesis, Properties and Applications. *J. Colloid Interface Sci.* **2015**, *447*, 217–228.

(16) Huo, C.; Li, M.; Huang, X.; Yang, H.; Mann, S. Membrane Engineering of Colloidosome Microcompartments Using Partially Hydrophobic Mesoporous Silica Nanoparticles. *Langmuir* **2014**, *30*, 15047–15052.

(17) Gao, J.; Wang, Y.; Du, Y.; Zhou, L.; He, Y.; Ma, L.; Yin, L.; Kong, W.; Jiang, Y. Construction of Biocatalytic Colloidosome Using Lipase-Containing Dendritic Mesoporous Silica Nanospheres for Enhanced Enzyme Catalysis. *Chem. Eng. J.* **2017**, *317*, 175–186.

(18) Mishra, A.; Price, H.; Patil, A. J.; Mann, S. Dynamic Co-clustering and Self-sorting in Interactive Protocell Populations. *Angew. Chem., Int. Ed.* **2024**, *64*, e202420209.

(19) Binks, B. P.; Lumsdon, S. O. Pickering Emulsions Stabilized by Monodisperse Latex Particles: Effects of Particle Size. *Langmuir* **2001**, *17*, 4540–4547.

(20) Dinsmore, A. D.; Hsu, M. F.; Nikolaides, M. G.; Marquez, M.; Bausch, A. R.; Weitz, D. A. Colloidosomes: Selectively Permeable Capsules Composed of Colloidal Particles. *Science* **2002**, *298*, 1006–1009.

(21) Shah, R. K.; Kim, J.-W.; Weitz, D. A. Monodisperse Stimuli-Responsive Colloidosomes by Self-Assembly of Microgels in Droplets. *Langmuir* **2010**, *26*, 1561–1565.

(22) Guan, X.; Liu, Y.; Xia, Y.; Tse, Y. L. S.; Ngai, T. Assembly and Jamming of Polar Additive-Swollen Microgels at Liquid–Liquid Interfaces: From Inverse Pickering Emulsions to Functional Materials. *J. Colloid Interface Sci.* **2025**, *679*, 284–293.

(23) Kwok, M.; Ngai, T. A Confocal Microscopy Study of Micron-Sized Poly(N-Isopropylacrylamide) Microgel Particles at the Oil-Water Interface and Anisotopic Flattening of Highly Swollen Microgel. *J. Colloid Interface Sci.* **2016**, *461*, 409–418.

(24) Toor, R.; Copstein, A. N.; Trébuchet, C.; Goudeau, B.; Garrigue, P.; Lapeyre, V.; Perro, A.; Ravaine, V. Responsive Microgels-Based Colloidosomes Constructed from All-Aqueous PH-Switchable Coacervate Droplets. *J. Colloid Interface Sci.* **2023**, *630*, 66–75.

(25) Jung, S. H.; Meyer, F.; Hörnig, S.; Bund, M.; Häßel, B.; Guerzoni, L. P. B.; De Laporte, L.; Messaoud, G. B.; Centeno, S. P.; Pich, A. On-Chip Fabrication of Colloidal Suprastructures by Assembly and Supramolecular Interlinking of Microgels. *Small* **2023**, *20*.

(26) Tamate, R.; Ueki, T.; Yoshida, R. Evolved Colloidosomes Undergoing Cell-like Autonomous Shape Oscillations with Buckling. *Angew. Chem., Int. Ed.* **2016**, *55*, 5179–5183.

(27) Destribats, M.; Lapeyre, V.; Sellier, E.; Leal-Calderon, F.; Schmitt, V.; Ravaine, V. Water-in-Oil Emulsions Stabilized by Water-Dispersible Poly(N-Isopropylacrylamide) Microgels: Understanding Anti-Finkle Behavior. *Langmuir* **2011**, *27*, 14096–14107.

(28) Rasmusson, M.; Routh, A.; Vincent, B. Flocculation of Microgel Particles with Sodium Chloride and Sodium Polystyrene Sulfonate as a Function of Temperature. *Langmuir* **2004**, *20*, 3536–3542.

(29) Fanaian, S.; Al-Manasir, N.; Zhu, K.; Kjøniksen, A.-L.; Nyström, B. Effects of Hofmeister Anions on the Flocculation Behavior of Temperature-Responsive Poly(N-Isopropylacrylamide) Microgels. *Colloid Polym. Sci.* **2012**, *290*, 1609–1616.

(30) Matsui, S.; Inui, K.; Kumai, Y.; Yoshida, R.; Suzuki, D. Autonomously Oscillating Hydrogel Microspheres with High-Frequency Swelling/Deswelling and Dispersing/Flocculating Oscillations. *ACS Biomater. Sci. Eng.* **2019**, *5*, 5615–5622.

(31) Yoshikawa, K. Distinct Activation Energies for Temporal and Spatial Oscillations in the Belousov-Zhabotinskii Reaction. *Bull. Chem. Soc. Jpn.* **1982**, *55*, 2042–2045.

463

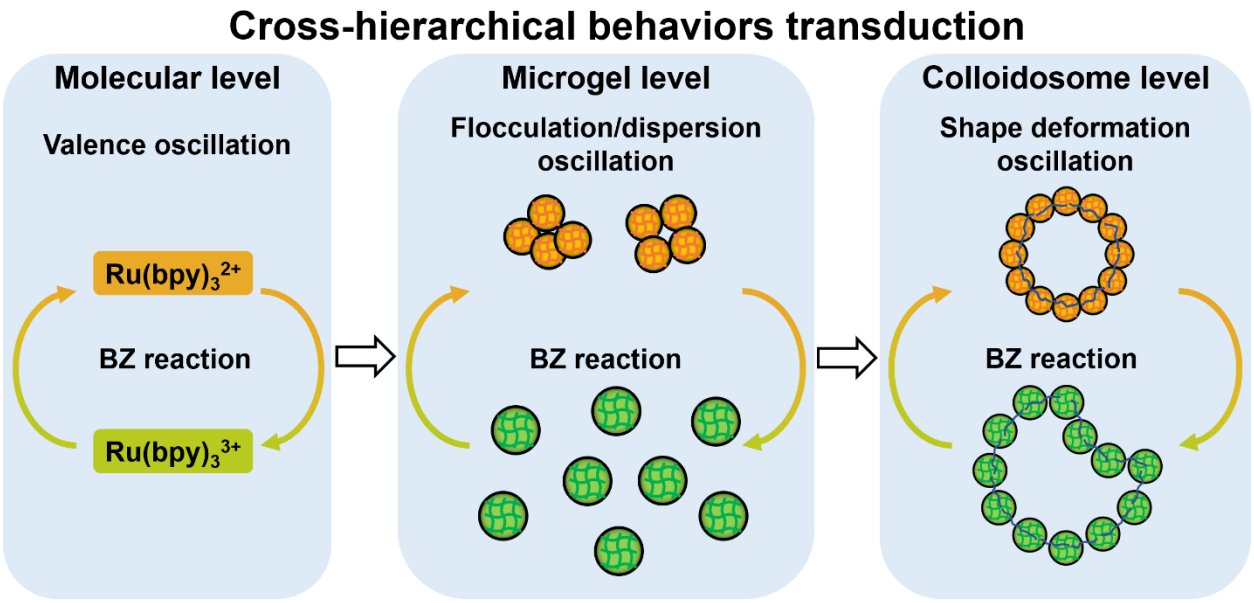

464

465 TOC